IEEE Access
Multidisciplinary : Rapid Review : Open Access Journal

Received November 28, 2020, accepted January 8, 2021, date of publication January 12, 2021, date of current version January 22, 2021.

Digital Object Identifier 10.1109/ACCESS.2021.3051180

3D Rapid-Prototyped 21-31-GHz Hollow SIWs for Low-Cost 5G IoT and Robotic Applications

GIORGOS SAVVIDES[1], NATTAPONG DUANGRIT[2], (Member, IEEE), NONCHANUTT CHUDPOOTI[3], (Member, IEEE), PRAYOOT AKKARAEKTHALIN[4], (Member, IEEE), ULRIK IMBERG[5], IAN D. ROBERTSON[1], (Fellow, IEEE), AND NUTAPONG SOMJIT[1], (Senior Member, IEEE)

[1]School of Electronic and Electrical Engineering, University of Leeds, Leeds LS2 9JT, U.K.
[2]Faculty of Engineering, Rajamangala University of Technology Lanna, Chiang Mai 50300, Thailand
[3]Research Center of Innovation Digital and Electromagnetic Technology (iDEMT), Department of Industrial Physics and Medical Instrumentation, Faculty of Applied Science, King Mongkut's University of Technology North Bangkok, Bangkok 10800, Thailand
[4]Department of Electrical and Computer Engineering, Faculty of Engineering, King Mongkut's University of Technology North Bangkok, Bangkok 10800, Thailand
[5]Huawei Technologies Sweden AB, 16440 Kista, Sweden

Corresponding author: Nutapong Somjit (n.somjit@leeds.ac.uk)

This work was supported in part by the Thailand Research Fund and Office of the Higher Education Commission through the Research Grant for New Scholar under Grant MRG6280119, in part by the King Mongkut's University of Technology North Bangkok under Contract KMUTNB-64-KNOW-44, and in part by the Engineering and Physical Science Research Council under Grant EP/S016813/1 and Grant EP/N010523/1.

ABSTRACT This article presents, for the first time, new design and fabrication techniques for Hollow Substrate Integrated Waveguides (HSIWs), demonstrated in the nominal frequency from 21 to 31 GHz, for use in wireless communication applications such as 5G, IoT and robotics. The design and fabrication techniques introduced in this paper feature: 1) the use of low-cost rapid prototyping additive manufacturing based on polymer jetting (PJ), and 2) the use of commercially available through-substrate copper via transitions. In contrast to the conventional SIW designs and fabrications, this new approach does not rely on through-substrate via fabrication, hence avoiding some difficult manufacturing steps, such as through-substrate etching, via formation and via metallization, which are considered complex and expensive to implement. The 3D printed HSIWs in this article can achieve a propagation loss of lower than 1.56 Np/m (13.55 dB/m), which is considered one of the results with the lowest propagation loss achieved to date, when compared to the state-of-the-art.

INDEX TERMS Substrate integrated waveguide, millimeter waves, additive manufacturing.

I. INTRODUCTION

Transmission lines are crucially important in many high frequency applications and are used in RF, microwave, millimeter-wave (mmWave) and terahertz systems. There are many types of transmission line structures such as rectangular waveguide (RWG), coaxial cable, microstrip line, stripline, coplanar waveguide (CPW) and, more recently, substrate integrated waveguide (SIW) [1]–[8]. RWGs generally provide many advantages compared to the other conventional transmission line types, such as extremely low propagation loss, high power-handling capability and superior measurement repeatability for many precision test applications. However, they are relatively bulky and cannot easily be integrated with active devices and integrated circuits to realize wireless communications transceivers in mass production. Coaxial lines are widely used as interconnections between high frequency components/devices working up to a few hundreds of GHz but they are also not suitable for integration with high frequency integrated circuits and subsystems such as RFICs or MMICs [1], [3]. Microstrip and CPW are extensively used in integrated circuit technologies because they provide a low-cost and planar solution, are simple to fabricate, and convenient for integration with both passive and active circuit devices [4]–[8]. Recently, SIWs have attracted a great deal of research interest and industrial development because they combine these advantages with some of the performance capabilities of RWG: They have low physical

The associate editor coordinating the review of this manuscript and approving it for publication was Kuang Zhang.

This work is licensed under a Creative Commons Attribution 4.0 License. For more information, see https://creativecommons.org/licenses/by/4.0/

profile, high Q-factor, good power-handling capability and are easy to integrate with other planar circuits, active devices and integrated circuits [9]– [11].

SIWs can outperform other planar transmission line technologies, such as microstrip or CPW, because of their lower propagation loss and higher power-handling capability. Moreover, microstrip and CPW structures have undesired electromagnetic (EM) radiation and usually suffer from signal dispersion at millimeter-wave and terahertz frequencies, which can significantly degrade the efficiency and performance of functional components [12]–[15]. In [16], SIW is shown to have similar propagation characteristics and performance when compared to the conventional RWG. The mode of electromagnetic (EM) wave propagation inside an SIW resembles that used in a conventional RWG. Its loss mechanisms are similar and loss is attributed to three factors: finite metal conductivity (α_c), dielectric loss (α_d) and radiation leakage (α_r).

There are two main types of SIW that have been reported during the last decade [17]–[20]: 1) dielectric-filled, which is most common, and 2) hollow substrate integrated waveguide (HSIW). In [20], a slot antenna demonstrated based on a dielectric-filled SIW structure using the electrodeposition fabrication was presented. It consists of very thin and closely spaced metallic wires to reduce the leakage loss but the propagation loss was compromised due to the lossy dielectric substrate.

Generally, the main reason to select HSIWs over dielectric-filled SIWs is due to the dielectric loss of the substrate used to fill the waveguide cavity. There are many research works that developed the HSIW-based functional devices by removing the dielectric material inside the waveguide structures [21]–[29], e.g. by using a multi-layered printed circuit board (PCB) structures. Moreover, the HSIWs can preserve many advantages inherited from SIWs and RWG, such as high level of system and circuit integration as well as high Q-factor and high power-handling capability [30], [31]. In [23], HSIW was used in a multilayer U-band phase shifter, fabricated using a standard PCB process, showing a significant improvement in the attenuation; from 40 dB/m to only 12.2 dB/m. Similarly, in [24], an air-filled SIW (AFSIW) fabricated using a standard multilayer PCB process, with a lossy FR-4 substrate, was demonstrated at 27-40 GHz and achieved a measured attenuation constant as low as 0.51 Np/m (4.43 dB/m).

In general, air-filled SIWs have low transmission losses but require more complex manufacturing processes and are particularly dependent on through-substrate via-hole fabrication which implies higher fabrication cost. For example, the HSIWs in [25] and [26] used very costly low-temperature co-fired ceramic (LTCC) processes, which suffer from high fabrication and material costs as well as thermal shrinkage of substrates, drastically reducing the fabrication reliability and accuracy. In [26], an average attenuation constant of as low as 17.37 dB/m or 2 Np/m was reported. In [27], an ‘‘empty’’ SIW was demonstrated with an exceptional transmission loss of 0.8 Np/m at 19.5 GHz by completely removing all dielectric material in the structure using the standard PCB fabrication process. However, all reported HSIWs used PCB, LTCC or similar fabrication techniques that rely heavily on through-substrate transitions and vias, resulting in higher manufacturing cost and a complex fabrication process, especially at millimeter-wave frequencies and beyond. In [32], the metallic vertical walls of the traditional SIW were replaced by using a Bragg structure, reducing the overall propagation loss but the fabrication method is complex and the fabrication costs are comparatively large.

This article presents a novel design and fabrication approach for realizing HSIW at low cost by using a simple fabrication process that combines two manufacturing techniques: 1) additive manufacturing based on polymer jetting (PJ), and 2) integration of commercially-available prefabricated through-substrate copper via transitions. The 3D-printed HSIWs demonstrated in this article cover the operational frequency range from 21 to 32 GHz, which covers many of the wireless communication frequency bands used for 5G, IoT and robotics. The novel design and fabrication approach has several advantages when compared to conventional fabrication techniques such as PCB, LTCC and cleanroom processes. Firstly, additive manufacturing techniques have been proven to be very useful for the low-cost rapid-prototyping of high-frequency components from only a few MHz to THz [33]–[38]. Secondly, by using the commercially available prefabricated through-substrate via transitions, the manufacturing of through vias can be massively simplified, which is in contrast to the conventional fabrication processes that require many complicated fabrication steps such as through-substrate etching, via forming and electroplating to metallize the through-substrate via-holes. Thirdly, since the through-substrate vias are already prefabricated, the reliability of the through-substrate vias and the fabrication of the vias are highly reliable, resulting in high fabrication yields.

II. ANALYSIS, DESIGN AND FABRICATION

A. STATE-OF-THE-ART 3D PRINTING TECHNIQUES

As comprehensively reported [39], 3D printing techniques are generally classified into five categories: fused deposition modeling (FDM), stereolithography apparatus (SLA), digital light processing (DLP), selective laser sintering (SLS), and polymer jetting (PJ).

The FDM technique uses thermoplastic materials, which come in filament form. This technique constructs the model by depositing the melted filaments along pre-determined paths. This technique results in the lowest printing resolution and high surface roughness. The standard layer heights of a single printed path range from 50 to 500 μm, which is limited by the nozzle size and the viscosity of the filament materials. However, material-extrusion based 3D printing techniques such as FDM are known to suffer voids within the printed parts [40].

The SLA and DLP techniques use a light source to pattern a 3D structure by selectively curing resin-based photopolymer. The light sources of the SLA and DLP techniques are a laser beam and an ultraviolet light, respectively. The resolution of these techniques depends on the spot size used to pattern the 3D structure. The best printing resolutions of the structure height for the SLA and DLP techniques are typically 25 μm and 1 μm, respectively. A surface roughness of less than 10 μm can be achieved by these techniques.

The SLS technique patterns a polymeric powder material layer-by-layer using a high-intensity laser beam for selective sintering. The best printing resolution for the SLS technique is typically 20 μm for the structure height. The printing resolution depends on the microparticle size of the powder material. However, this technique has a very limited choice of materials for the microparticle powders, limiting its use for microwave and mm-wave applications.

The PJ technique provides the best printing accuracy and resolutions compared with the other four techniques. This technique is like inkjet printing because it uses a nozzle head to drop liquid photopolymer onto the printing area. The photopolymer materials are cured by UV light to create the 3D patterned structure step-by-step. The best printing resolution is approximately 14 μm for the structure height. The surface roughness is less than 10 μm.

For this work, the PJ technique was selected for fabricating the HSIW because this technique provides the best printing accuracy and resolution and offers the smallest surface roughness, while still achieving low fabrication cost.

B. THEORETICAL ANALYSIS AND DESIGN

The detailed geometry of the novel 3D printed HSIW is depicted in Fig. 1. Fig. 1(a) represents the 3D exploded view of the HSIW structure consisting of four different parts: (1) the commercially prefabricated through-substrate copper via transitions, (2) the top copper sheet being laser-patterned and containing the microstrip feeds and microstrip-to-SIW transitions as well as circular etch-hole array, (3) the 3D printed substrate using standard acrylonitrile butadiene styrene (ABS), and (4) the laser-patterned bottom copper sheet with circular etch-hole array and microstrip grounds. Fabricated into the top copper sheet, 50-ohm microstrip lines are used as EM-mode transitions between the 2.4-mm coaxial connectors and the HSIW structures which have a characteristic impedance of 48-ohm [41]. The bottom copper sheet was also laser-patterned and contains the ground planes of the microstrip transitions and the circular etch-hole array to form the HSIW metal fence posts. The standard ABS 3D-printing material, with a dielectric constant, ε_r, of 2.75 and a loss tangent, tan δ, of 0.025 [39], [42]–[44], was used to fabricate the hollow substrate structure sandwiched with two aforementioned laser-patterned copper sheets on the top and bottom of the substrate. The substrate thickness, T_s, was selected to be 0.5 mm for the 3D-printed HSIWs, which is matched to the thickness of the readymade copper via transitions and

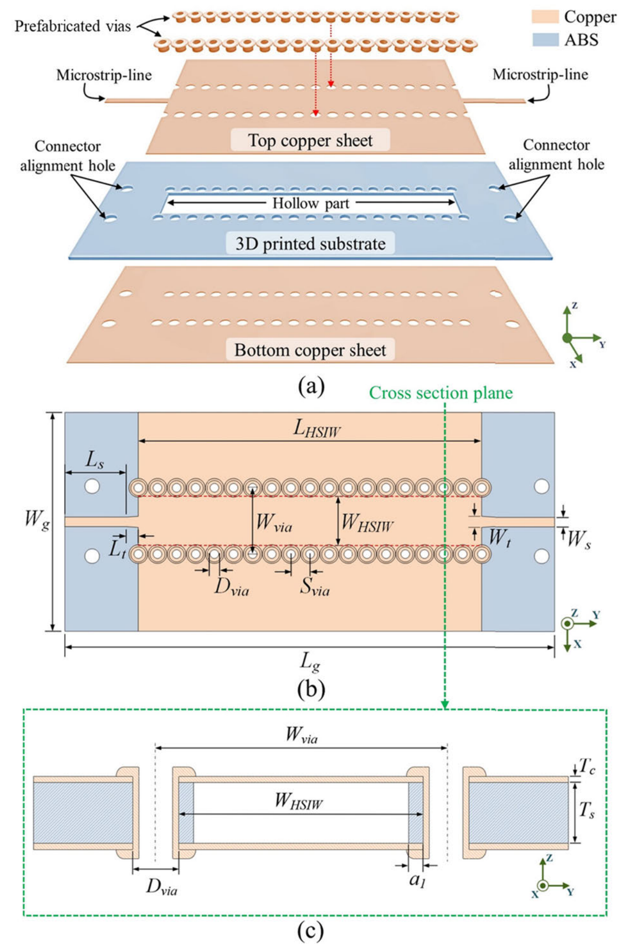

FIGURE 1. Schematic diagrams of the novel HSIW in this paper: (a) 3D exploded view, (b) top view with all design parameter, and (c) cross-sectional view of the HSIW.

offers ease of impedance matching between the microstrip transition and the HSIWs.

Commercially prefabricated through-copper via transitions were used to assemble and firmly attach all three previously fabricated parts by using the Through Hole Mechanical Press [45]. Figures 1(b) and 1(c), represent the top view and the cross-sectional view of the 3D-printed HSIW, respectively. The values of the design parameters are shown in Table 1. The HSIW structure and all microstrip transitions are designed and optimized by using the 3D full-wave EM simulation package CST Studio Suite [46]. The 3D-printed HSIW in this article was optimized for the operating frequency range of 21-31 GHz, which is suitable for many applications in high-speed 5G, IoT and robotic communications.

In [25], the theoretical analysis is investigated for the propagation mode inside a HSIW, which is an EM combination between the conventional RWG and SIW structures. The effect of the dielectric portion inside a hollow waveguide can be determined by defining a loading ratio, q, as shown in equation (1):

$$q = \frac{2a_1\sqrt{\varepsilon_r}}{W_{HSIW}} \quad (1)$$

TABLE 1. The Design Parameters of the HSIWs.

Parameter	Description	Value (mm)
W_s	Width of microstrip line	1.2
W_t	Width of a taper transition from microstrip line to HSIW	1.3
W_{via}	Distance between vias centers	9.0
W_{HSIW}	Width of HSIW	6.6
L_s	Length of microstrip line	8.0
L_t	Length of taper transition	2.0
L_{HSIW}	Length of HSIW	46.8, 52.0, 91.0
D_{via}	Diameter of via hole	1.2
S_{via}	Spacing between vias	2.6
T_c	Thickness of copper sheet	0.15
T_s	Substrate thickness	0.5
a_1	Width of the dielectric filling inside the HSIW	0.4

where a_1 is the width of the dielectric filling inside the hollow SIW as shown in Fig. 1(c), ε_r is the dielectric constant of the substrate material, and W_{HSIW} is the width of the HSIW structure. The lower the value of q, the more the structure behaves like the conventional RWG. According to [25], the maximum value of q used to design the HSIW should be lower than 0.35. The q of the 3D-printed HSIW was carefully determined by considering the fabrication resolution of the 3D printer used in this work, which can provide the minimum a_1 of 0.4 mm and, therefore, the q value of 0.175 is calculated by using equation (1). The cutoff frequency of the 3D-printed HSIW is chosen to be 21 GHz to provide the operational frequency range of 21 to 31 GHz. Therefore, the W_{HSIW} can be calculated by using equation (2): where c_0 is the velocity of light in free space and f_c is the cutoff frequency (Hz):

$$W_{HSIW} = \frac{c_0}{2f_c\left[0.999 + 4.946 \times 10^{-4} \times e^{(9.406q)}\right]} \quad (2)$$

$$S_{via} \geq H_{via} \quad (3)$$

The readymade through-copper vias used in this work are offered by Fortex and have an outer diameter of 1.6 mm and an inner diameter, D_{via}, of 1.2 mm [45]. The cap of the prefabricated copper vias have a diameter, H_{via}, of 2.6 mm, therefore, the minimum spacing between two adjacent vias, S_{via}, can be calculated and chosen using equation (3), so the caps of the prefabricated vias will not collide with each other after fabrication. To minimize EM leakage losses through the substrate (α_r), the optimum space of 2.6 mm between two adjacent vias, S_{via}, was chosen.

Figure 2 illustrates the simulated electric field (E-filed) of the 3D-printed HSIW with a length of 46.8 mm at a frequency of 26 GHz, which is the center frequency of the selected frequency band. The ratio between the maximum guided E-field inside the hollow of the HSIW and maximum leaked E-field into the substrate of 7.275×10^{-3} is calculated, implying that the leaked E-field of the 3D-printed HSIW can be neglected.

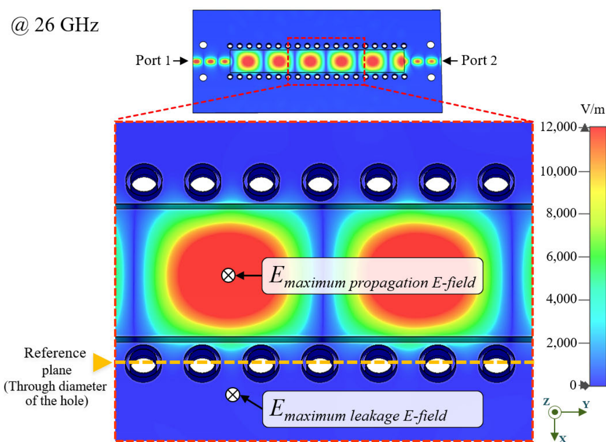

FIGURE 2. Electric field distribution at 26 GHz inside the proposed HSIW with the length of 46.8 mm.

An effective dielectric constant, ε_e, is a virtual dielectric parameter that combines the material properties of air and the dielectric substrate of the partially loaded RWG [25], [26]. The effective dielectric constant, ε_e, is calculated as follows:-

$$\varepsilon_e = \varepsilon_0 \varepsilon_{r,eff}(1 - j\tan\delta_{eff}) \quad (4)$$

where, ε_0, which is permittivity of free space, is 8.85×10^{-12} F·m^{-1}, $\varepsilon_{r,eff}$ is effective relative permittivity and tan δ_{eff} is effective loss factor. As in [25] and [26], to calculate the effective dielectric constant, ε_e, it is necessary to first calculate the value of the effective permittivity, $\varepsilon_{r,eff}$, and the normalized effective loss factor, tan δ_n, as in equations (5) and (6):

$$\varepsilon_{r,\,eff} = \frac{\beta^2 + \left(\frac{\pi}{W_{HSIW}}\right)^2}{k_0^2} \quad (5)$$

$$\tan\delta_n = \frac{\tan\delta_{eff}}{\tan\delta} = \frac{\varepsilon_r}{\varepsilon_{r,eff}}\left[1 + \frac{k_{x1}^2}{k_{x2}^2}\frac{a_2 + \sin(k_{x2}a_2)/k_{x2}}{a_1 - \sin(k_{x1}a_2)/k_{x1}}\frac{\cos^2(k_{x1}a_1/2)}{\sin^2(k_{x2}a_2/2)}\right]^{-1} \quad (6)$$

where, a_1 is the width of the dielectric filling inside the HSIW and a_2 is the width of the air filling inside the HSIW, which can be calculated from $a_2 = W_{HSIW} - 2a_1$. The k_{x1} and k_{x2} are the x-direction wavenumber inside the HSIW in the dielectric and air, respectively.

The calculated effective relative permittivity, $\varepsilon_{r,eff}$, and normalized effective loss factor, tan δ_n, of the 3D-printed HSIW are plotted in Fig. 3, which shows that $\varepsilon_{r,eff}$ varies from 1.00309 to 1.00337 and tan δ_n varies from 5.64×10^{-3} to 6.80×10^{-3} for the whole single-mode operating band. The trend is for $\varepsilon_{r,eff}$ and tan δ_n to increase with frequency towards the end of the single propagation mode at $f/f_c = 2$. The plots in Fig. 3 indicate that the values of $\varepsilon_{r,eff}$ and the tan δ_n are close to an air-filled structure. The effective

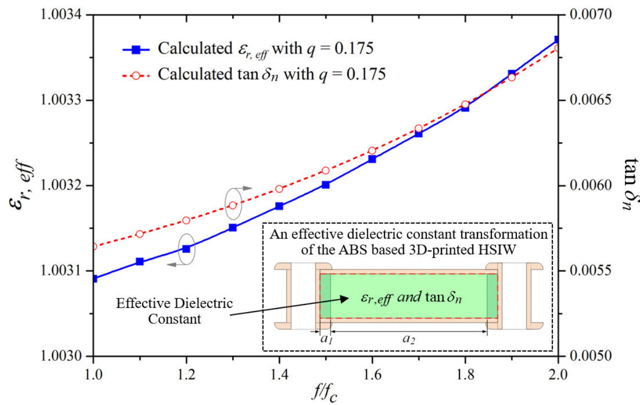

FIGURE 3. Calculated effective relative permittivity, $\varepsilon_{r,eff}$, of the loaded RWG with two dielectric materials, which are air and ABS with the dielectric constant of 2.75, following Eqn. (5) and the normalized effective loss factor, tan δ_n, following Eqn. (6).

TABLE 2. List of Material Properties Used in Transmission Line Simulations.

Material	Dielectric constant	Loss tangent (tan δ)
ABS	2.75	0.025
Roger RT5880	2.2	0.0009
High resistivity silicon	11.9	0.001

dielectric constant, $\varepsilon_{r,eff}$, is nearly equal to one and the normalized effective loss factor, tan δ_n, gives a negligible angle value.

C. DESIGN COMPARISON

As illustrated in Fig. 4(a)-(c), a comprehensive design study investigating the figure of merit of different planar transmission lines was conducted and supported by EM simulations comparing conventional structures, e.g. microstrip and CPW, with the 3D printed HSIW. Commonly used substrate materials for microstrip lines and CPWs, such as Roger RT5880 and high resistivity silicon (with resistivity more than 4 kΩ-cm), were chosen and compared to ABS for their propagation characteristics. The material properties used in all transmission line simulations are presented in Table 2. The AWR TX-LINE is used to preliminary calculate the dimensions of microstrip and CPW structures before conducting the 3D full-wave simulations [47]. The multiline calculation technique is employed to extract the attenuation and phase constants through the simulated S-parameters. Therefore, at least two different lengths of each transmission line are required and simulated [48], [49]. Figure 4(d) shows the simulated attenuation constant of the 3D-printed HSIW compared with the conventional planar transmission lines, both microstrips and CPWs. Microstrip transmission lines, simulated with substrate materials of standard ABS, RT5880, and HRS achieve average attenuation constants of 9.480 Np/m (82.29 dB/m), 0.622 Np/m (5.39 dB/m), and 0.863 Np/m (7.49 dB/m), respectively, in the frequency range from 21 GHz to 31 GHz. The CPW designs with the same substrate materials have attenuation constants of 5.037 Np/m (43.72 dB/m), 0.397 Np/m (3.45 dB/m), and 0.418 Np/m (3.63 dB/m) using ABS, RT5880, and HRS, respectively. Although the microstrip and CPW transmission line designs using ABS substrates have higher signal attenuations as compared to the designs using RT5880 and HRS, the ABS substrate does not show any significant increase in attenuation constant for the HSIW case. From Fig. 4(d), all microstrip transmission lines and CPWs clearly suffer from both radiation and material losses when the frequency increases, while this is not the case for the 3D-printed HSIWs. Moreover, even though some microstrip and CPW designs using RT5880 and HRS substrates exhibit slightly lower attenuation constant compared to the ABS-based HSIW, these substrate materials are normally at least 100x more expensive compared to ABS.

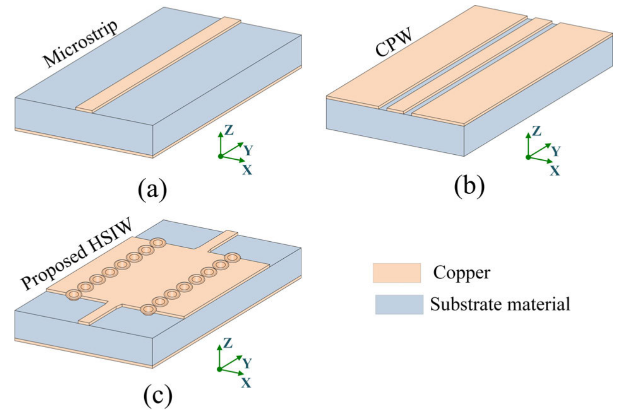

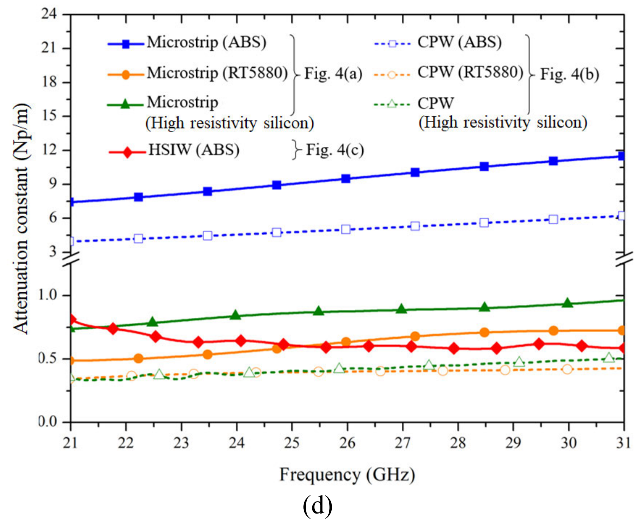

FIGURE 4. 3D views of the transmission line geometries used to compare their figure of merit in this work: (a) conventional microstrip line, (b) standard coplanar waveguide, (c) 3D-printed HSIW, and (d) the extracted attenuation constant of the all aforementioned transmission lines with different substrate materials (simulated).

D. HSIW FABRICATION AND ASSEMBLY

Figure 5(a) shows the fabricated HSIW component parts for the length of 46.8-mm. There is a laser-patterned top and

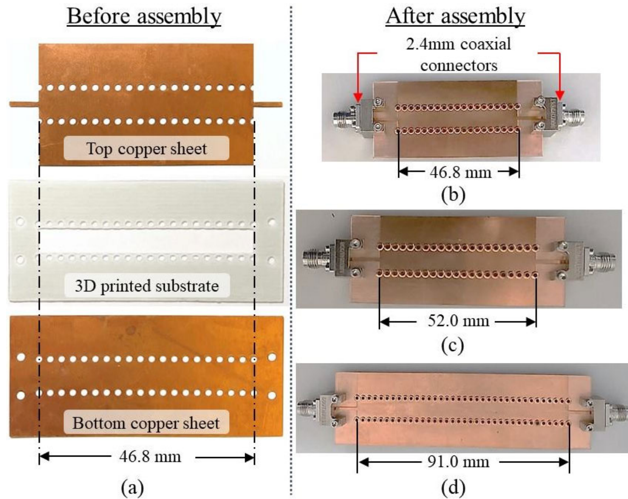

FIGURE 5. Fabricated HSIW prototype before and after assembly. (a) The 3D-printed HSIW is composed of the top and bottom laser-patterned copper sheets containing microstrip feed transitions and HSIW etch-hole array, and 3D printed ABS substrate with the total length of 46.8 mm. The right hand pictures show the fabricated HSIW after assembly with three different lengths of (b) 46.8 mm, (c) 52.0 mm, and (d) 91.0 mm, mounted with relaunchable 2.4-mm coaxial connectors at the end of microstrip feed lines.

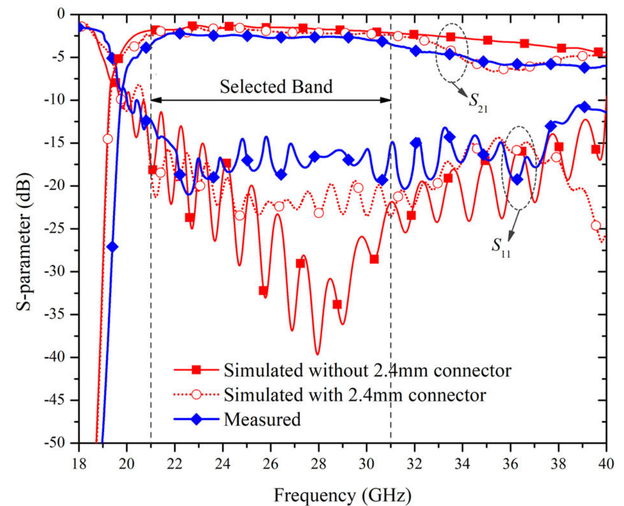

FIGURE 6. Simulated and measured S -parameters of the 91.0 mm-long 3D-printed HSIW over the operational band of 21-31 GHz. The plot also shows the effect of the 2.4mm coaxial connectors on the S-parameters (simulated).

bottom copper sheet and the 3D printed waveguide substrate formed of ABS. Figure 5(b)-5(d) show the manufactured and assembled HSIW prototypes of three different HSIW designs with lengths of 46.8 mm, 52.0 mm, and 91.0 mm, respectively. First, the top and bottom copper sheets are made of a 99.9%-purity copper sheet with the thickness of 0.15 mm [50]. The sheets were cut into the desired shapes by using the water laser cutting technology (Laser-MicroJet Cutter) to form the microstrip feeds and matching transitions as well as circular etched-hole arrays [51]. For the 3D printed substrate, Stratasys Object1000 3D printer is used to fabricate the substrate of the HSIW with ABS material [52]. The whole fabrication process is considered a very cost-effective precision manufacturing compared to other fabrication methods as summarized in [53].

The ABS-based HSIW structure was assembled by using commercial ready-to-use through-copper via transitions to firmly attach all fabricated copper and ABS layers together, avoiding the utilization of the complicated and costly conventional via and through-substrate fabrication process, e.g. through-substrate etching, electroplating for through via metallization and wet etching using various chemicals. The ABS-based HSIW structure is mechanically attached and fixed between the top and bottom copper sheets by using commercial ready-to-use through-copper via transitions. The commercial prefabricated through-copper via array is mechanically compressed by using the mechanical PCB through-hole-plating press tool [45], firmly fixing all the SIW parts together. Moreover, four screws are used to further fixing the SIW parts, shown in Fig. 5(b). These screw holes are also used as the connector alignment hole to accurately align each part of the SIW together. The final assembled 3D printed HSIW prototypes are shown in Fig. 5(b)-5(d) with the length of 46.8 mm, 52.0 mm, and 91.0 mm, respectively.

III. MEASUREMENT RESULTS

All three HSIW prototypes were attached with relaunchable SOUTHWEST 2.4-mm coaxial connectors mounted on both sides of the microstrip feed lines. The S-parameters were measured using Agilent E8361A PNA Microwave Network Analyzer with two-port Short-Open-Load-Through (SOLT) calibration, bringing the S-parameter reference plane to the ends of the coaxial cables used for further coaxial connector terminations. The frequency range was set to 15 GHz – 40 GHz on the PNA with 3201 frequency points. Figure 6 compares the measured and simulated reflection, S_{11}, and transmission coefficients, S_{21}, of the fabricated HSIW prototype with the length of 91.0 mm. The measured reflection coefficient, S_{11}, of the 3D-printed HSIW was lower than -10 dB over the operational band of 21–31 GHz while the S_{21} is better than -3.56 dB for the entire selected band. Fig. 6 also shows the effect of the 2.4mm coaxial connectors on the S-parameters of the 3D printed HSIW. However, since the multiline technique is used to calculate the transmission line loss, the effect of the coaxial connectors is removed after the mathematical calculations.

By using the multiline calculation technique [48], [49], the phase and attenuation constants of the 3D-printed HSIWs can be extracted from the measured and simulated S-parameters as shown in Fig. 7. Over the whole operational band from 21 – 31 GHz, the average attenuation constant extracted from the simulated results without and with 2.4-mm coaxial connectors are 0.629 Np/m and 0.636 Np/m, respectively, while the measured attenuation constant has an average value of 1.56 Np/m. The main reasons for the propagation loss difference come from the fact that the dielectric and metal materials used in the designs are more lossy.

TABLE 3. Key Parameters Comparison of Measurement Results of This Work With Other Published Work.

Key parameters	[24]	[26]	[28]	[29]	*This work*
Structure	Air-filled SIW[1] (AFSIW)	Hollow SIW (HSIW)	Dielectric-filled SIW (DFSIW)	Half-mode SIW (HMSIW)	***Hollow SIW (HSIW)***
Operating frequency	26.5 − 40 GHz	26.5 − 40 GHz	20 − 40 GHz	26.5 − 40 GHz	***21 − 31 GHz***
Fractional bandwidth	40.60 %	40.60 %	66.67 %	40.60 %	***38.46 %***
Substrate material	Roger 6002	LTCC[2]	Roger 5880	Roger 6002	***ABS (3D printed)***
Fabrication process	PCB + Laser micromachining lapping and polishing sputtering	Progressive-lamination LTCC	PCB + Laser micromachining or mechanical CNC[3] micromilling	Mechanical CNC[3] micromilling	***3D printing technology + laser-microjet cutter***
Via hole fabrication	Electroplating	Conductive paste with Progressive-lamination	Electroplating	Electroplating	***Commercial prefabricated through copper vias***
Fabrication complexity	Moderate	Difficult	Simple	Moderate	***Simple***
Transition	CBCPW[4] to SIW and SIW to AFSIW	RWG to HSIW	ML[5] to DFSIW	ML to HMSIW	***ML to HSIW***
Propagation constant	0.51 Np/m	2 Np/m	2.5 Np/m	1.75 Np/m	***1.56 Np/m***
Fabrication cost	Medium	High	Medium	Medium	***Low***
Substrate and material costs	High	High	High	High	***Low***

[1]SIW: substrate integrated waveguide; [2]LTCC: low temperature co-fired ceramic; [3]CNC: computerized numerical control; [4]CBCPW: conductor-backed coplanar waveguide; [5]ML: microstrip line.

Also, the electrical connections between the patterned copper sheets and prefabricated through-substrate copper vias are not perfect. Specifically, during the assembly process, the ready-to-use through-copper vias were placed one-by-one into the etch-hole arrays of the copper sheets and, subsequently, attached to the HSIW structure. Then, commercial prefabricated copper vias were pressed with the mechanical PCB through-hole-plating press machine, which slightly affect the copper via shape due to the slightly high manually pressing force. Fortunately, this fabrication process can be further optimized and automated in the future. Even with some minor fabrication and assembly issues, the 3D-printed HSIWs can achieve the average signal propagation loss of 1.56 Np/m, which is among the lowest attenuation loss published to date. In Fig. 7, the extracted phase constant of the measured S-parameter results is also plotted and compared to the one calculated from the simulations with and without the 2.4-mm coaxial connectors.

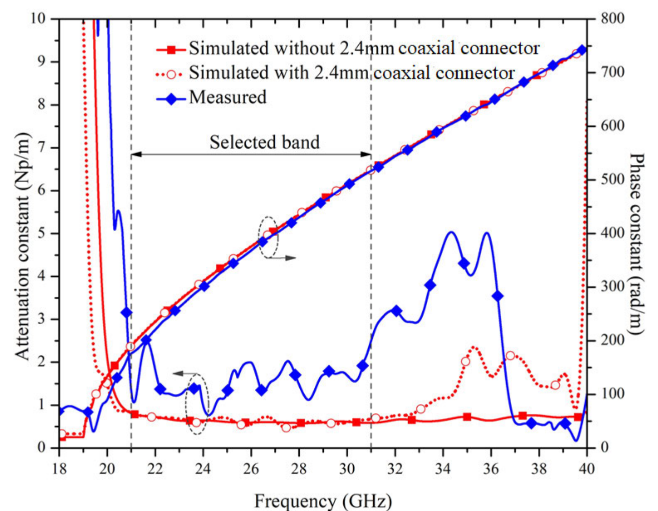

FIGURE 7. Extracted propagation characteristics of the 3D-printed HSIW comparing phase and attenuation constants calculated from the measured and simulated S-parameters over the nominal frequency band from 21-31 GHz.

Table 3 presents the key parameter comparisons between the 3D-printed HSIW with other state-of-the-art SIW designs with a similar frequency range recently reported [24], [26], [28], [29]. The substrate material used in this work is standard ABS, which is inexpensive when compared with the other commercially-available microwave substrate materials in [24], [26], [28], [29], e.g., Roger 5880, Roger 6002 and LTCC. In [24], [28], [29], the fabrication process uses a CNC/Laser micro-milling machine to manufacture the devices, which are comparatively expensive compared with 3D printing technology. Moreover, most of SIW fabrications

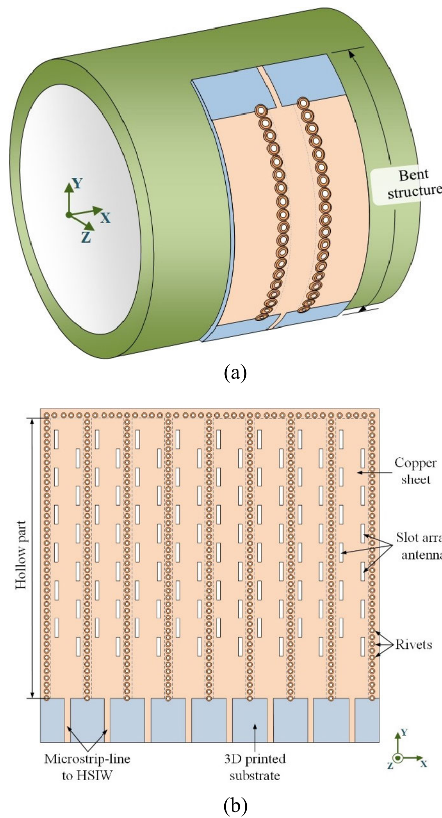

FIGURE 8. Potential applications of the HSIW: (a) HSIW conformal structure used as a communication medium on the arm of a robot and (b) MIMO HSIW slotted array antenna using in the 5G/6G communication systems.

rely critically on the fabrication of the through-substrate vias and via metallization, which are normally very complicated and costly, especially at high frequencies. The new idea in combining 3D printing technology and using commercial prefabricated through-substrate vias eliminates the aforementioned issues, e.g. fabrication complexity and overall development costs, and, thus, opens a new opportunity in developments of very low cost and less complex high frequency integrated components and devices for many applications such as 5G, IoT and high speed robotic communications.

IV. POTENTIAL APPLICATIONS

As presented in this article, the performance of the HSIW using 3D printing technology to fabricate the hollow substrate channels is excellent. It has advantages of stability, broadband design, low-cost, low-profile design, lightweight, and the possibility for mechanical flexibility. It offers a new degree of design freedom for applications benefitting from the use of conformal and flexible structures, which are now very easy to fabricate compared with the conventional rectangular waveguide structure.

Thus, the 3D-printed HSIW can be used in flexible conformal structures, such as in robotic communication systems where multiple transceiver RF chains are required and the antennas are to be integrated into the mechanical body.

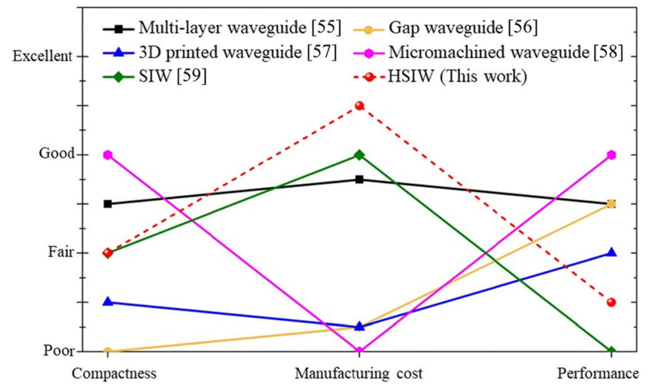

FIGURE 9. A comparison of emerging waveguide technologies in terms of compactness, manufacturing cost, and RF performance as presented in [54].

An example application is shown in Figure 8(a), illustrating a flexible HSIW structure that could be used as a communication device on the arm of a robot. This HSIW can be potentially designed with a flexible substrate, instead of the rigid ABS material used for this work and therefore it can be bent at an angle and wrapped around a conformal structure e.g. a cylindrical shape.

Moreover, since 5G communication networks utilize MIMO technology, this HSIW technology can be used to implement antenna arrays. As illustrated in Figure 8(b), the HSIW could be potentially used to realise a slot antenna array in a MIMO configuration. The MIMO slot antenna array provides enhanced gain and narrow beam width, giving new design flexibility and compatibility with integrated circuits and other planar PCB circuits in millimeter wave applications.

V. CONCLUSION

This article has described a novel methodology for the fabrication of millimeter-wave HSIW structures based on 3D printing of the substrate, combined with laser cutting of the conductors and pre-formed via-hole plugs. The measured attenuation constant of the 3D-printed HSIW is less than 1.56 Np/m over the operating frequency range of 21-31 GHz, and a fractional bandwidth of 38.46% is achieved. The 3D-printed HSIW is compact, low cost, broadband, low loss, and easy to fabricate and integrate with other planar circuits. The measured results of the 3D-printed HSIW show that the device can be applied to be used for 5G communication with easy integration of other RF passive and active components such as filter, combiner/splitter, and antenna. Figure 9 presented a comparison of key novel waveguide technologies along with our proposed HSIW, in terms of three key factors; compactness, manufacturing cost, and performance [54]. There are five emerging waveguide (WG) technologies presented in the graph; the multi-layer waveguide [55], gap waveguide [56], 3D printed waveguide [57], micromachined waveguide [58], and SIW [59] compared with the 3D-printed HSIW. The 3D-printed HSIW in this work has a compactness similar to the SIW techniques and

a better performance and lower manufacturing cost than the SIW. Although the 3D-printed HSIW has a slightly worse performance compared with the 3D printed waveguide technique, overall the 3D-printed HSIW has low manufacturing cost compared to the other technologies. This work has proved the concept, but further work is required to further optimize the fabrication process. The authors will seek to optimize and develop the fabrication steps, such as reducing the thickness of copper sheet [60], using automatic via-fabrication [61] and reducing the loss from the 3D-printed substrate [62], [63] in future work.

REFERENCES

[1] D. M. Pozar, *Microwave Engineering*, 4th ed. Hoboken, NJ: Wiley, 2012.

[2] I. D. Robertson, N. Somjit, and M. Chongcheawchamnan, *Microwave and Millimetre-Wave Design for Wireless Communication*. Hoboken, NJ, USA: Wiley, 2016.

[3] T. Kai, "A coaxial line to post-wall waveguide transition for a cost-effective transformer between a RF-device and a planar slot-array antenna in 60-GHz band," *IEICE Trans. Commun.*, vols. E89–B, no. 5, pp. 1646–1653, May 2006.

[4] J. Coonrod and B. Rautio, "Comparing microstrip and CPW performance," *Microw. J.*, vol. 55, no. 7, pp. 74–86, Jul. 2012.

[5] E. C. Niehenke, R. A. Pucel, and I. J. Bahl, "Microwave and millimeter-wave integrated circuits," *IEEE Trans. Microw. Theory Techn.*, vol. 50, no. 3, pp. 846–857, Mar. 2002.

[6] W. Deal, "Coplanar waveguide basics for MMIC and PCB design," *IEEE Microw. Mag.*, vol. 9, no. 4, pp. 120–133, Aug. 2008.

[7] M. Abulghasim, J. Tabatchnick, and M. Markovic, "Comparison of embedded coplanar waveguide and strip line for multi-layer boards," Semantic Scholar, Seattle, WA, USA, Tech. Rep., 2019. Accessed: Jan. 30, 2020. [Online]. Available: https://www.semanticscholar.org/paper/Comparison-of-Embedded-Coplanar-Waveguide-and-for-Abulghasim-Tabatchnick/82e09d51ca4d0ca992f9f5cc6a5c3854b7fc4ab9

[8] Y. CPW Yun, H. S. Kim, and N. Jang, "Study on characteristics of various RF transmission line structure on PES substrates for application to flexible MMIC," *ETRI J.*, vol. 36, no. 1, pp. 1646–1653, Feb. 2014.

[9] D. Deslandes and K. Wu, "Integrated microstrip and rectangular waveguide in planar form," *IEEE Microw. Wireless Compon. Lett.*, vol. 11, no. 2, pp. 68–70, Feb. 2001.

[10] M. Bozzi, A. Georgiadis, and K. Wu, "Review of substrate-integratedwaveguide circuits and antennas," *IET Microw., Antennas Propag.*, vol. 5, no. 8, pp. 909–920, 2011.

[11] H. Kumar, "A Review on Substrate Integrated Waveguide and its Microstrip Interconnect," *IOSR J. Electron. Commun. Eng.*, vol. 3, no. 5, pp. 36–40, 2012.

[12] K. Wu, D. Desiandes, and Y. Cassivi, "The substrate integrated circuits-a new concept for high-frequency electronics and optoelectronics," in *Proc. 6th Int. Conf. Telecommun. Modern Satell., Cable Broadcast. Service*, Nis, Yugoslavia, 2003, p. 3.

[13] X.-P. Chen and K. Wu, "Low-loss ultra-wideband transition between conductor-backed coplanar waveguide and substrate integrated waveguide," in *IEEE MTT-S Int. Microw. Symp. Dig.*, Boston, MA, USA, Jun. 2009, pp. 349–352.

[14] L. Jin, R. M. Lee, and I. D. Robertson, "Analysis and design of a slotted waveguide antenna array using hollow substrate integrated waveguide," in *Proc. Eur. Microw. Conf. (EuMC)*, Paris, France, Sep. 2015, pp. 1423–1426.

[15] M. Bozzi, M. Pasian, and L. Perregrini, "Modeling of losses in substrate integrated waveguide components," in *Proc. Int. Conf. Numer. Electromagn. Model. Optim. for RF, Microw., Terahertz Appl. (NEMO)*, Pavia, Italy, May 2014, pp. 1–4.

[16] M. Bozzi, C. Tomassoni, L. Perregrini, R. Bahr, and M. Tentzeris, "Additive manufacturing of substrate integrated waveguide components," in *IEEE MTT-S Int. Microw. Symp. Dig.*, Chengdu, China, Jul. 2016, pp. 1–4.

[17] D. Deslandes and K. Wu, "Accurate modeling, wave mechanisms, and design considerations of a substrate integrated waveguide," *IEEE Trans. Microw. Theory Techn.*, vol. 54, no. 6, pp. 2516–2526, Jun. 2006.

[18] E. Diaz-Caballero, A. Belenguer, H. Esteban, V. E. Boria, C. Bachiller, and J. V. Morro, "Analysis and design of passive microwave components in substrate integrated waveguide technology," in *IEEE MTT-S Int. Microw. Symp. Dig.*, Ottawa, ON, Canada, Aug. 2015, pp. 1–3.

[19] Y. Li, L.-A. Yang, L. Du, K. Zhang, and Y. Hao, "Design of millimeter-wave resonant cavity and filter using 3-D substrate-integrated circular waveguide," *IEEE Microw. Wireless Compon. Lett.*, vol. 27, no. 8, pp. 706–708, Aug. 2017.

[20] H. Yousef, S. Cheng, and H. Kratz, "Substrate integrated waveguides (SIWs) in a flexible printed circuit board for millimeter-wave applications," *J. Microelectromech. Syst.*, vol. 18, no. 1, pp. 154–162, Feb. 2009.

[21] N. Ranjkesh and M. Shahabadi, "Reduction of dielectric losses in substrate integrated waveguide," *Electron. Lett.*, vol. 42, no. 21, pp. 1230–1231, Oct. 2006.

[22] F. Bigelli, D. Mencarelli, M. Farina, G. Venanzoni, P. Scalmati, and C. Renghini, "Design and fabrication of a dielectric substrate-integrated waveguide," *IEEE Trans. Compon., Packag., Manuf. Technol.*, vol. 6, no. 2, pp. 256–261, Feb. 2016.

[23] F. Parment, A. Ghiotto, T.-P. Vuong, J.-M. Duchamp, and K. Wu, "Air-filled SIW transmission line and phase shifter for high-performance and low-cost U-Band integrated circuits and systems," in *Proc. Global Symp. Millimeter-Waves (GSMM)*, Montreal, QC, Canada, May 2015, pp. 1–3.

[24] F. Parment, A. Ghiotto, T.-P. Vuong, J.-M. Duchamp, and K. Wu, "Air-filled substrate integrated waveguide for low-loss and high power-handling millimeter-wave substrate integrated circuits," *IEEE Trans. Microw. Theory Techn.*, vol. 63, no. 4, pp. 1228–1238, Apr. 2015.

[25] L. Jin, R. M. A. Lee, and I. Robertson, "Analysis and design of a novel low-loss hollow substrate integrated waveguide," *IEEE Trans. Microw. Theory Techn.*, vol. 62, no. 8, pp. 1616–1624, Aug. 2014.

[26] L. Jin, "Waveguide-based antenna arrays in multi-chip module technology," Ph.D. dissertation, School Electron. Elect. Eng., Univ. Leeds, Leeds, U.K., 2014.

[27] A. Belenguer, H. Esteban, and V. E. Boria, "Novel empty substrate integrated waveguide for high-performance microwave integrated circuits," *IEEE Trans. Microw. Theory Techn.*, vol. 62, no. 4, pp. 832–839, Apr. 2014.

[28] X.-C. Zhu, W. Hong, K. Wu, K.-D. Wang, L.-S. Li, Z.-C. Hao, H.-J. Tang, and J.-X. Chen, "Accurate characterization of attenuation constants of substrate integrated waveguide using resonator method," *IEEE Microw. Wireless Compon. Lett.*, vol. 23, no. 12, pp. 677–679, Dec. 2013.

[29] I. S. S. Lima, F. Parment, A. Ghiotto, T.-P. Vuong, and K. Wu, "Broadband Dielectric-to-Half-Mode air-filled substrate integrated waveguide transition," *IEEE Microw. Wireless Compon. Lett.*, vol. 26, no. 6, pp. 383–385, Jun. 2016.

[30] Y. Dong, P. Liu, D. Yu, B. Yi, and G. Li, "Active substrate integrated terahertz waveguide using periodic graphene stack," *AIP Adv.*, vol. 5, no. 11, Nov. 2015, Art. no. 117237.

[31] K. Wu, Y. Jian Cheng, T. Djerafi, and W. Hong, "Substrate-integrated millimeter-wave and terahertz antenna technology," *Proc. IEEE*, vol. 100, no. 7, pp. 2219–2232, Jul. 2012.

[32] B. Hong, N. Feng, J. Chen, G. Wang, V. Doychinov, R. Clarke, J. Cunningham, I. Robertson, and N. Somjit, "Substrate integrated Bragg waveguide: An octave-bandwidth single-mode hybrid transmission line for millimeter-wave applications," *Opt. Exp.*, vol. 28, pp. 27903–27918 (2020).

[33] C. Guo, X. Shang, J. Li, M. J. Lancaster, and J. Xu, "3-D printed lightweight microwave waveguide devices," in *Proc. IEEE 5th Asia–Pacific Conf. Antennas Propag. (APCAP)*, Kaohsiung, Taiwan, Jul. 2016, pp. 47–48.

[34] B. T. Malik, V. Doychinov, S. A. R. Zaidi, I. D. Robertson, and N. Somjit, "Antenna gain enhancement by using low-infill 3D-printed dielectric lens antennas," *IEEE Access*, vol. 7, pp. 102467–102476, 2019.

[35] N. Chudpooti, S. Praesomboon, N. Duangrit, N. Somjit, and P. Akkaraekthalin, "An X-band portable 3D-printed lens antenna with integrated waveguide feed for microwave imaging," in *Proc. Photon. Electromagn. Res. Symp. (PIERS-Spring)*, Rome, Italy, Jun. 2019, pp. 487–492.

[36] N. Chudpooti, N. Duangrit, P. Akkaraekthalin, I. D. Robertson, and N. Somjit, "220-320 GHz hemispherical lens antennas using digital light processed photopolymers," *IEEE Access*, vol. 7, pp. 12283–12290, 2019.

[37] N. Chudpooti, N. Duangrit, P. Akkaraekthalin, I. D. Robertson, and N. Somjit, "Electronics-based free-space terahertz measurement using hemispherical lens antennas," *IEEE Access*, vol. 7, pp. 95536–95546, 2019.

[38] B. T. Malik, V. Doychinov, S. A. R. Zaidi, I. D. Robertson, N. Somjit, R. Richardson, and N. Chudpooti, "Flexible rectennas for wireless power transfer to wearable sensors at 24 GHz," in *Proc. Res., Invention, Innov. Congr. (RI2C)*, Bangkok, Thailand, Dec. 2019, pp. 1–5, doi: 10.1109/RI2C48728.2019.8999964.

[39] N. Duangrit, B. Hong, A. D. Burnett, P. Akkaraekthalin, I. D. Robertson, and N. Somjit, "Terahertz dielectric property characterization of photopolymers for additive manufacturing," *IEEE Access*, vol. 7, pp. 12339–12347, 2019.

[40] G. L. Goh, S. Agarwala, G. D. Goh, H. K. J. Tan, L. Zhao, T. K. Chuah, and W. Y. Yeong, "Additively manufactured multi-material free-form structure with printed electronics," *Int. J. Adv. Manuf. Technol.*, vol. 94, nos. 1–4, pp. 1309–1316, Jan. 2018.

[41] D. Deslandes, "Design equations for tapered microstrip-to-Substrate integrated waveguide transitions," in *IEEE MTT-S Int. Microw. Symp. Dig.*, Anaheim, CA, USA, May 2010, pp. 704–707.

[42] C.-K. Lee, J. McGhee, C. Tsipogiannis, S. Zhang, D. Cadman, A. Goulas, T. Whittaker, R. Gheisari, D. Engstrom, J. Vardaxoglou, and W. Whittow, "Evaluation of microwave characterization methods for additively manufactured materials," *Designs*, vol. 3, no. 4, p. 47, Sep. 2019.

[43] J. Pourahmadazar and T. A. Denidni, "Author correction: Towards millimeter-wavelength: Transmission-mode fresnel-zone plate lens antennas using plastic material porosity control in homogeneous medium," *Sci. Rep.*, vol. 8, no. 1, Dec. 2018, Art. no. 5300.

[44] H. Xin and M. Liang, "3-D-printed microwave and THz devices using polymer jetting techniques," *Proc. IEEE*, vol. 105, no. 4, pp. 737–755, Apr. 2017.

[45] FORTEX. *PTH400 Mechanical Through Hole Press*. Accessed: Mar. 30, 2020. [Online]. Available: http://www.fortex.co.uk/download/pth400-mechanical-through-hole-press/

[46] *CST-MW Studio*, Comput. Simul. Technol., Framingham, MA, USA, 2017.

[47] Cadence Design Systems. *Transmission-line calculator (TX-Line Software)*. Accessed: Feb. 10, 2020. [Online]. Available: https://www.awr.com/awr-software/options/tx-line

[48] M. D. Janezic and J. A. Jargon, "Complex permittivity determination from propagation constant measurements," *IEEE Microw. Guided Wave Lett.*, vol. 9, no. 2, pp. 76–78, Feb. 1999.

[49] F. Xu and K. Wu, "Guided-wave and leakage characteristics of substrate integrated waveguide," *IEEE Trans. Microw. Theory Techn.*, vol. 53, no. 1, pp. 66–73, Jan. 2005.

[50] Goodfellow. *Supplier for Materials*. Accessed: Apr. 2, 2020. [Online]. Available: http://www.goodfellow.com/

[51] Synova. *MCS 300 Laser-MicroJet Cutter*. Accessed: Jul. 4, 2020. [Online]. Available: www.synova.ch/machines/mcs-series/

[52] Stratasys Company. *3D Printing & Additive Manufacturing*. Accessed: Jul. 10, 2020. [Online]. Available: https://www.stratasys.com

[53] A. Belenguer, H. Esteban, A. L. Borja, and V. E. Boria, "Empty SIW technologies: A major step toward realizing low-cost and low-loss microwave circuits," *IEEE Microw. Mag.*, vol. 20, no. 3, pp. 24–45, Mar. 2019.

[54] Ericson. (May 2020). *Making Waves: A New Method for mmWave Antennas and Components*. [Online]. Available: https://www.ericsson.com/en/blog/2020/5/new-method-for-millimeter-wave-antennas

[55] A. Vosoogh, H. Zirath, and Z. S. He, "Novel air-filled waveguide transmission line based on multilayer thin metal plates," *IEEE Trans. THz Sci. Technol.*, vol. 9, no. 3, pp. 282–290, May 2019.

[56] E. Rajo-Iglesias, M. Ferrando-Rocher, and A. U. Zaman, "Gap waveguide technology for millimeter-wave antenna systems," *IEEE Commun. Mag.*, vol. 56, no. 7, pp. 14–20, Jul. 2018.

[57] A. Tamayo-Dominguez, J.-M. Fernandez-Gonzalez, and M. Sierra-Perez, "Metal-coated 3D-printed waveguide devices for mm-Wave applications [Application Notes]," *IEEE Microw. Mag.*, vol. 20, no. 9, pp. 18–31, Sep. 2019.

[58] A. Gomez-Torrent and J. Oberhammer, "Micromachined waveguide interposer for the characterization of multi-port sub-THz devices," *J. Infr., Millim., THz Waves*, vol. 41, no. 3, pp. 245–257, Mar. 2020.

[59] L. Sun, H.-W. Deng, Y.-F. Xue, J.-M. Zhu, and S.-B. Xing, "Compact-balanced BPF and filtering crossover with intrinsic common-mode suppression using single-layered SIW cavity," *IEEE Microw. Wireless Compon. Lett.*, vol. 30, no. 2, pp. 144–147, Feb. 2020.

[60] I. E. Obuh, V. Doychinov, D. P. Steenson, P. Akkaraekthalin, I. D. Robertson, and N. Somjit, "Low-cost microfabrication for MEMS switches and varactors," *IEEE Trans. Compon., Packag., Manuf. Technol.*, vol. 8, no. 9, pp. 1702–1710, Sep. 2018.

[61] S. J. Bleiker, A. C. Fischer, U. Shah, N. Somjit, T. Haraldsson, N. Roxhed, J. Oberhammer, G. Stemme, and F. Niklaus, "High-aspect-ratio through silicon vias for high-frequency application fabricated by magnetic assembly of gold-coated nickel wires," *IEEE Trans. Compon., Packag., Manuf. Technol.*, vol. 5, no. 1, pp. 21–27, Jan. 2015, doi: 10.1109/TCPMT.2014.2369236.

[62] N. Somjit, G. Stemme, and J. Oberhammer, "Binary-coded 4.25-bit W-band Monocrystalline–Silicon MEMS multistage dielectric-block phase shifters," *IEEE Trans. Microw. Theory Techn.*, vol. 57, no. 11, pp. 2834–2840, Nov. 2009, doi: 10.1109/TMTT.2009.2032350.

[63] P. Kadam, A. Odhekar, and A. A. Deshmukh, "Air suspended multiband E-Shaped microstrip antenna," in *Proc. 4th Int. Conf. Comput. Commun. Control Autom. (ICCUBEA)*, Pune, India, Aug. 2018, pp. 1–6.

GIORGOS SAVVIDES was born in Nicosia, Cyprus, in 1993. He received the M.Eng. degree (Hons.) in electronics engineering from the University of Leeds, Leeds, U.K., in 2018, where he is currently pursuing the Ph.D. degree, supported by EPSRC DTP Scholarship. His current research interest includes millimetre-wave circuits and devices.

NATTAPONG DUANGRIT (Member, IEEE) received the B.Eng. degree in electronics and telecommunication engineering from the Rajamangala University of Technology Thanyaburi (RMUTT), in 2014, and the Ph.D. degree from the King Mongkut's University of Technology North Bangkok (KMUTNB), Bangkok, Thailand, in 2019. His Ph.D. was supported by the Thailand Research Fund through the Royal Golden Jubilee Ph.D. Program. His current research interests include the application of 3D printing technology for millimeter-wave and THz devices, and substrate integrated waveguide applications.

NONCHANUTT CHUDPOOTI (Member, IEEE) received the B.Sc. degree (Hons.) in industrial physics and medical instrumentation and the Ph.D. degree in electrical engineering from the King Mongkut's University of Technology North Bangkok, in 2012 and 2018, respectively. He was a Lecturer with the Department of Industrial Physics and Medical Instrumentation, Faculty of Applied Science, King Mongkut's University of Technology North Bangkok, in 2018. His current research interests include the application of microwave microfluidic sensors, millimeter-wave substrate integrated circuit applications, and substrate integrated waveguide applications. He was a recipient of the Best Presentation Award from the Thailand-Japan Microwave, in 2015 and 2018, and the Young Researcher Encouragement Award, in 2016.

PRAYOOT AKKARAEKTHALIN (Member, IEEE) received the B.Eng. and M.Eng. degrees in electrical engineering from the King Mongkut's University of Technology North Bangkok (KMUTNB), Bangkok, Thailand, in 1986 and 1990, respectively, and the Ph.D. degree from the University of Delaware, Newark, DE, USA, in 1998. From 1986 to 1988, he was a Research and Development Engineer with Microtek Products Co., Ltd., Thailand. In 1988, he joined the Department of Electrical Engineering, KMUTNB. He was the Head of the Senior Research Scholar Project which was supported by the Thailand Research Fund, from 2015 to 2017. He has authored or coauthored more than 40 international journals, more than 200 conference papers, and four books/book chapters. His current research interests include RF/microwave circuits, wideband and multiband antennas, telecommunication, and sensor systems. He is a member of IEICE, Japan, ECTI, and the EEAAT Association, Thailand. He was the Chairman of the IEEE MTT/AP/ED Thailand Joint Chapter, from 2007 to 2010, and the Vice President and the President of the ECTI Association, Thailand, from 2012 to 2013 and from 2014 to 2015, respectively. He was the Editor-in-Chief of ECTI Transactions, from 2011 to 2013.

ULRIK IMBERG received the M.Sc. degree in applied physics and electrical engineering from the Institute of Technology, Linköping University, in 1997. He is currently leading the Wireless Technology Planning Team, Huawei Technologies Sweden AB. His research interests include 5G& 6G telecommunication systems & technologies, especially active antennas and antenna-near electronics and photonics.

IAN D. ROBERTSON (Fellow, IEEE) received the B.Sc. (Eng.) and Ph.D. degrees from King's College London, London, U.K., in 1984 and 1990, respectively. From 1984 to 1986, he was with the GaAs MMIC Research Group, Plessey Research, Caswell, U.K. In 1986, he returned to King's College, initially as a Research Assistant working on the T-SAT project and, then, as a Lecturer leading the MMIC Research Team, where he became a Reader in 1994. In 1998, he became a Professor of microwave subsystems engineering with the University of Surrey, where he established the Microwave Systems Research Group and was a Founding Member of the Advanced Technology Institute. In 2004, he was appointed as the Centenary Chair in microwave and millimetre-wave/circuits with the University of Leeds. He was the Director of learning and teaching, from 2006 to 2011, and the Head of the school, from 2011 to 2016.

Dr. Robertson was the General Technical Programme Committee Chair of the European Microwave Week, in 2011 and 2016.

NUTAPONG SOMJIT (Senior Member, IEEE) received the Dipl.-Ing. (M.Sc.) degree from the Dresden University of Technology, in 2005, and the Ph.D. degree from the KTH Royal Institute of Technology, in 2012. In 2012, he returned to the Dresden University of Technology to lead a research team in micro-sensors and MEMS ICs for the Chair for Circuit Design and Network Theory. In 2013, he was appointed as a Lecturer (Assistant Professor) with the School of Electronic and Electrical Engineering, University of Leeds. His current research interests include integrated smart high-frequency components, heterogeneous integration, and low-cost microfabrication processes.

Dr. Somjit has been a member of the International Editorial Board of the *International Journal of Applied Science and Technology*, since 2013. He was appointed as a member of the Engineering, Physical and Space Science Research Panel of the British Council, in 2014. He was a recipient of the Best Paper Award (EuMIC prize) from the European Microwave Week, in 2009. He received a Graduate Fellowship from the IEEE Microwave Theory and Techniques Society, in 2010 and 2011, and the IEEE Doctoral Research Award from the IEEE Antennas and Propagation Society, in 2012. In 2016, he was the Chair of the Student Design Competition for the European Microwave Week. In 2018, he was appointed as an Associate Editor of *Electronics Letters* (IET).